International Journal of Biological Macromolecules 272 (2024) 132804

Contents lists available at ScienceDirect

International Journal of Biological Macromolecules

journal homepage: www.elsevier.com/locate/ijbiomac

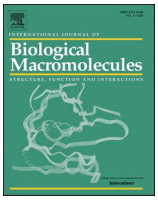

Cellulose from dinoflagellates as a versatile and environmentally friendly platform for the production of functionalised cellulose nanofibres

Amina Alizade [a,*], Tobias Reich [b], Anne Jantschke [a]

[a] Biomineralization/Crystallography, Institute of Geosciences, Johannes Gutenberg University Mainz, J.-J.-Becher-Weg 21, D-55128 Mainz, Germany
[b] Department of Chemistry – Nuclear Chemistry, Johannes Gutenberg University Mainz, Fritz-Strassmann-Weg 2, 55128 Mainz, Germany

ARTICLE INFO

Keywords:
CNF
TEMPO oxidation
Amine grafting
Microalgae
Drug delivery

ABSTRACT

Cellulose nanofibres (CNFs), also known as nano-fibrillated cellulose, have emerged as highly promising sustainable biomaterials owing to their numerous advantages, including high accessibility, long-term sustainability, low toxicity, and mechanical properties. Recently, marine organisms have been explored as novel and environmentally friendly sources of cellulose fibers (CFs) due to their easy cultivation, extraction and biocompatibility. Dinoflagellates, a group of marine phytoplankton, have gained particular attention due to their unique cellulosic morphology and lignin-free biomass. Previously, we showed that the unique amorphous nature of dinoflagellate-derived cellulose offers various benefits. This study further explores the potential of dinoflagellate-derived CFs as a sustainable and versatile CNF source. Extracted dinoflagellate cellulose is effectively converted into CNFs via one-step TEMPO oxidation without significant polymer degradation. In addition, the biological compatibility of the CNFs is improved by amine-grafting using putrescine and folic acid. The products are characterised by conductometric titration, zeta potential measurements, TGA, GPC, FTIR, SEM/TEM, XRD, and XPS. Finally, in a proof-of-principle study, the application of the functionalised CNFs in drug delivery is tested using methylene blue as a drug model. Our findings suggest that dinoflagellate-derived CNFs provide an eco-friendly platform that can be easily functionalised for various applications, including drug delivery.

1. Introduction

Cellulose nanofibres (CNFs), also known as nano-fibrillated cellulose, have emerged as a highly promising sustainable biomaterial owing to their numerous advantages, including high accessibility, long-term sustainability, low toxicity, and useful mechanical properties [1–5]. The biocompatibility of cellulose-based nanomaterials makes them a particularly suitable candidate for many applications, such as in reinforcement materials, sensors, air and water filters, or biomedical applications (e.g., drug delivery) [2,6–10]. For instance, highly crystalline CNFs are used as a reinforcing material due to their high tensile strength (10 GPa) [11]. CNF aerogels are demonstrated to be effective air filters (e.g., for particulate matter or CO_2) due to their high specific surface area [5,12]. The potential of cellulose-based materials, especially CNFs, in water purification was reviewed by Azimi et al. [13]. The loading of CNFs with active compounds enables additional functionalities: For instance, CNF-immobilised Prussian blue exhibits a remarkable ability to selectively trap radioactive Cs contamination in soil and seawater [14]. Doxorubicin-loaded CNF thin films were able to reduce the number of pancreatic cancer cells in model studies [15].

Native cellulose fibres (CFs) are composed of repeating D-anhydrous glucose units (AGU) linked by a β-1,4-glycosidic bond that is reinforced by intrachain hydrogen bonds. Individual cellulose chains are connected via intermolecular hydrogen bonds to form a microfibril. To obtain CNFs, it is necessary to subject those native fibres to different purification and delamination methods (e.g., enzymatic hydrolysis, sulfonation, carboxymethylation, grinding, refining or blending) [1]. In general, the conversion of native microfibrils to nanoscale cellulose fibres combines several steps: (i) extraction of pure cellulose pulp (mechanical cellulosic biomass); (ii) (mechanical, biological or chemical) pre-treatment of pure cellulose pulp to facilitate fibre delamination; and (iii) mechanical disintegration of the fibres (cellulose bundles are completely broken down to individual fibrils) [1,4,16,17]. The number of these purification and delamination steps varies depending on the cellulose source [16–18].

Usually, animals and plants have been prioritised as cellulose sources due to their significant cellulose content (ranging from ~40 % to ~80 %) [19–21]. Nevertheless, because of their cultivation requirements and

* Corresponding author.
E-mail addresses: aalizade@uni-mainz.de (A. Alizade), jantschke@uni-mainz.de (A. Jantschke).

https://doi.org/10.1016/j.ijbiomac.2024.132804
Received 14 November 2023; Received in revised form 19 May 2024; Accepted 30 May 2024
Available online 31 May 2024

higher lignocellulosic biomass content (up to ~36 wt%) [18–20,22], obtaining pure cellulose pulp from these sources poses ecological concerns like arable land usage, deforestation, fertilisation and transportation costs, as well as multistep purification [19,21].

Alternative cellulose sources could be one option to reduce these problems [23–25]. Marine organisms (macro– and microalgae) are a promising alternative due to their abundant growth in a variety of habitats, including marine and freshwater environments, as well as in wastewater or lab cultures [25–28]. Several aspects make marine organisms particularly suitable as alternative cellulose sources: i) cultivation versatility and rapid growth; ii) high yields: a significant amount of biomass can be achieved in a short time and per unit area of cultivation; iii) low resource demands as they require only sunlight and CO_2; iv) cellulose diversity - from highly crystalline to fully amorphous cellulose; v) biodegradability; and vi) the possibility of tailoring properties through genetic engineering [25–28]. Overall, marine organisms provide a robust, innovative biomass for many applications.

Various types of macroalgae, such as *Ulva* sp., *Pasidonia oceanica*, *Valonia ventricose*, *Laminaria digitata*, and *Gelidium elegans*, have been comprehensively studied for cellulose extraction using methods like enzymatic hydrolysis, acid hydrolysis, and oxidation [28–31]. Extracting pure cellulose from macroalgae presents two significant challenges: First, due to the high lignin content in some macroalgae, such as *Pasidonia oceanica* (~30 wt%) and *Ulva* sp. (~10 wt%), multistep extraction methods must be used. Second, macroalgae-derived CFs (e.g., in *Siphonocladus* sp., *Apjohnia* sp., and *Chaetomorpha*) are highly crystalline, which requires additional hydrolysis and oxidation steps to break the inter- and intramolecular hydrogen bonds within the fibres [32,33]. For instance, a multi-step extraction and delamination procedure, including enzymatic hydrolysis, H_2SO_4 hydrolysis, and ultrasonication, was used to obtain CNFs from *Cladophora glomerata* and *Valonia ventricose* [31–33]. It is worth noting that such multistep extraction and delamination methods are wasteful and time-consuming.

Lately, microalgal-derived compounds, including cellulose, have been introduced as a promising alternative for application in bioengineering and biopolymer development [25,27,31,34,35]. With the exception of the work of Baba Hamed et al. [26] and Lee et al. [36], microalgae have not been extensively studied or utilised as a potential source of CNFs. Their works showed that CNFs can be produced from microalgae using TEMPO oxidation without any additional mechanical treatment [26,36]. Using 2 h of TEMPO oxidation at a pH of 10, they produced nanofibrils with a tensile strength of 3–4 GPa [26,36].

Recently, we have investigated one group of microalgae, namely the dinoflagellate species *Peridinium* sp. and *Prorocentrum micans* (*P. micans*), as a sustainable cellulose source [37]. These unicellular dinoflagellates have a cell-covering ('theca') made up of cellulose – the so-called armour or thecal plates [38,39]. These cellulosic thecal plates are established within amphiesmal vesicles during cell development and consist of randomly oriented fibres surrounded by a plasma membrane [38,39]. The cellulose theca of dinoflagellates is a superstructure of up to 30 individual, porous cellulose thecal plates connected by sutures. Each thecal plate has a unique pore structure.

We previously described the large-scale cultivation of the dinoflagellate species *Peridinium* sp. and *P. micans* (up to 20 l) and the isolation of pure amorphous cellulose using a simple extraction method at room temperature (RT) without disruption of the cellulose theca [37]. The resulting material is highly pure, lignin-free and composed mainly of amorphous CFs [37]. Its most important characteristics are summarised in the Materials and methods section.

When compared to other microalgae, dinoflagellate-derived cellulose is very pure and completely amorphous. As a result, the properties of dinoflagellate-derived cellulose differ significantly from those of other crystalline cellulose sources [27]. For example, the enhanced accessibility of the amorphous cellulose greatly simplifies cellulose extraction and functionalisation. These unique characteristics make dinoflagellate-derived cellulose an especially promising, sustainable and biocompatible candidate for biomedical applications.

The primary goal of this study is to demonstrate the superiority of amorphous dinoflagellate cellulose over other cellulose sources, i.e. other micro- and macroalgae, for the production of CNFs. We hypothesise that the use of dinoflagellate cellulose for the production of CNFs has several advantages: Due to its amorphous nature, the CNF production process is straightforward and requires less time, energy and chemicals.

Our research focuses on the development of a simple and robust protocol to convert extracted dinoflagellate CFs into biodegradable CNFs without the need for additional CF surface activation. To accomplish this, we are investigating the conversion of dinoflagellate-derived CFs to CNFs via a one-step oxidation protocol using TEMPO/NaOCl/NaBr. Subsequently, the biological affinity of the CNFs is increased by surface functionalisation with primary amine groups. Finally, in a proof-of-principle study, the potential of these functionalised CNFs for drug delivery is tested in vitro using methylene blue (MB) as a drug model.

The CNF formation, surface amine grafting and drug delivery properties of the materials are quantitatively and qualitatively characterised using ATR-FTIR, conductometric titration, UV–vis, zeta potential, GPC, XPS and SEM/TEM.

2. Materials and methods

2.1. Dinoflagellate cellulose source

Cellulose from the dinoflagellate species *Peridinium* sp. and *P. micans* was extracted at RT [37] and used as a source of natural CF. *Peridinium* sp. and *P. micans* were obtained from the Culture Collection Marburg (Dr. Stefan Zauner). *P. micans* is a marine species cultivated in medium f/2 [30,31], and *Peridinium* sp. is a freshwater species cultivated in medium Moor-Chu [32]. For cultivation details and comprehensive characterisation of this cellulose product, we refer the reader to our previous publications [37]. The primary characterisation of dinoflagellate-derived cellulose is: i) the cellulose yield is ~75 % (*w*/w) (pure cellulosic biomass/initial biomass, after removing all colour impurities, alongside proteins, lignin, hemicellulose, etc.); ii) Dinoflagellate cellulose is a predominantly amorphous cellulose II allomorph with a CrI <30 %; iii) $M_w \sim 20 \times 10^4$ g mol^{-1}; iv) the specific surface area is ~17 m^{2}g^{-1}; v) the material is thermally stable up to ~270 °C [37].

2.2. Chemicals

2,2,6,6-Tetramethylpiperidine-1-oxyl (TEMPO, 98 %) and methanol (MeOH, ≥99.99 %) were purchased from Sigma Aldrich. 1-Ethyl-3-(3-dimethylaminopropyl)-carbodiimide (EDC, 98+ %), N-Hydroxy succinimide (NHS, 98+ %), 1,4-diaminobuthane (putrescine, ≥99 %), folic acid (FA, 95–102 %), sodium hydroxide (NaOH), hydrogen chloride (HCl, 37 % Normapur), and lithium chloride (LiCl, Biotechnology grade) were purchased from VWR Chemicals. Sodium hypochlorite (NaOCl, 12 %, Biocide Grade) and methylene blue (MB, C.I. 52,015) were purchased from ROTH. Dimethylacetamide (DMAc, 99 %) and sodium bromide (NaBr, 99 %) were purchased from Thermo Scientific. Ethanol (EtOH, 99 %) was purchased from Fisher Chemicals. All chemicals were used without further purification.

2.3. TEMPO oxidation of algal cellulose

TEMPO oxidation of CF was performed by slightly modifying the well-established protocol by Isogai et al. [40]. About 200 mg of extracted CFs (an equivalent of ~1.23 mmol AGU) were suspended in 200 ml of double distilled water (DDW) and homogenised in an ultrasonic bath (Palssonic Profi) for 10 min. 39 mg (0.25 mmol) of TEMPO and 65 mg (0.63 mmol) of NaBr were suspended in 10 ml of DDW and added to the homogenised solution. After 5 min of stirring at 400 rpm, 0.8 ml of 12 % NaOCl (1:1 ratio of AGU/NaOCl) was added dropwise,

and the mixture was stirred for another hour (400 rpm, RT). The pH value of the reaction was maintained at pH 10 by adding 0.5 M NaOH. To analyse the effect of reaction time on the degree of oxidation, the reaction time was also prolonged to 12 h and 24 h while keeping the AGU/NaOCl-ratio constant.

At the end of oxidation, the reaction was quenched by adding 10 ml MeOH and then neutralised by adding 0.5 M NaOH to prevent further cellulose polymer degradation. To collect water-soluble CNFs after oxidation, an excess amount of EtOH (5–10 times the volume of reaction solution) was added to the solution, precipitated for 3 h, and collected by centrifugation (1920 rcf, 10 min). Then, the water-soluble product was washed 3 times using a 9/1 (v/v) EtOH/water mixture. Subsequently, the final product was freeze-dried (Christ, Alpha 1–4 LSC) and stored at 5 °C. The final product is designated as CNF_Tempo_1h, CNF_Tempo_12h and CNF_Tempo_24 h. The reaction scheme was illustrated in SI (Fig. S1).

2.4. Grafting of folic acid onto CNFs

Grafting of folic acid (FA) onto CNFs was conducted using 1-Ethyl-3-(3-dimethylaminopropyl)-carbodiimide/N-Hydroxysuccinimide (EDC/NHS) coupling similar to the procedure previously described by Shieh et al. [41]. The CNFs were initially modified with putrescine: 100 ml of 0.1 % (w/v) aqueous CNF solution was homogenised at 450 rpm for 10 min, then 1.5 eq. of NHS and 2 eq. of EDC were added to the suspension and stirred for 30 min. Following that, twice the equivalent of putrescine (2 mol-eq. per mol of carboxyl groups) was added and stirred while maintaining a pH of 7.5–8 at RT. The reaction continued overnight and was terminated by dropping pH to 1–2 using 0.1 M HCl to collect the putrescine-grafted sample. The product was washed via dialysis for 24–72 h using a cellulose dialysis membrane (ROTH, wd. 0.025 mm, br. 34 mm, MWCO 14000). The final product was collected by centrifugation (1920 rcf, 10 min) and lyophilisation (24 h). In the paper, this sample is designated as CNF_Tempo_24h_Putrescine. The reaction scheme of this process is illustrated in the SI (Fig. S2). The number of primary amine groups of the putrescine-modified CNFs was calculated using potentiometric-conductometric titration (SI, Figs. S9, S10, S11). Following that, 50 mg of dried putrescine-modified CNFs were mixed with 1.5 eq. of NHS and 2 eq. of EDC and stirred (450 rpm) for 30 min. Then, 2 eq. of FA was added and stirred for 24 h at RT while maintaining a reaction pH of 7.5–8. The reaction was terminated by dropping the pH to 1–2 using 0.1 M HCl. The product was washed using a cellulose dialysis membrane (ROTH, wd. 0.025 mm, br. 34 mm, MWCO 14000) for 24–72 h. The final product was collected by centrifugation (1920 rcf, 10 min) and lyophilisation (24 h). In the paper, this sample is designated as CNF_Tempo_24h_FA. The corresponding reaction scheme is illustrated in the SI (Fig. S3).

2.5. Drug loading and release

2.5.1. UV/Vis-spectroscopy

Drug loading efficiency (DLE) and drug release were analysed using MB as a model drug [42]. The amount of loaded MB was calculated from the absorption of the MB monomer at 665 nm [42] using a UV/Vis spectrophotometer (Analytik Jena, Specord® 50 Plus). Standard solutions of MB in the concentration range of 10^{-8} to 10^{-7} mol l^{-1} were prepared to obtain a standard calibration curve (SI, Fig. S15) used for linear regression. The MB monomer absorbance at 665 nm was chosen due to its stability in low concentrations.

2.5.2. Drug loading

20 ml of FA-grafted CNFs (1 g l^{-1}) were mixed with 20 ml of (400 mg l^{-1}) aqueous MB solution and gently rotated for 48 h while maintaining a pH of 8.5. After 48 h of mixing, the 1st supernatant was collected for UV/Vis analysis by centrifugation (1920 rcf, 10 min). The concentration of the residual MB in the supernatant was calculated from absorption at 665 nm.

2.5.3. Drug release

Drug release was studied in different phosphate buffers at pHs of 5.4, 6.7, and 7.4. 5 mg of MB-loaded dry cellulose samples were suspended in 13 ml of phosphate buffer while gently rotating for a total of 120 h. At hourly intervals, 0.5 ml aliquots were taken, and an identical volume of fresh buffer was added to the medium. The MB concentration in the aliquots was calculated from MB absorption at 665 nm.

3. Characterisation methods

3.1. Attenuated total reflectance-Fourier transform infrared spectroscopy (ATR-FTIR)

Samples were analysed by ATR-FTIR spectroscopy using a Thermo Scientific Nicolet 6700 equipped with a DTGS KBr detector and an attenuated total reflectance crystal accessory (ATR Golden Gate). FTIR spectra of dried cellulose were recorded between 4000 cm^{-1} and 400 cm^{-1} using 200 scans and a spectral resolution of 2 cm^{-1}. The obtained data were analysed using OMNIC™.

3.2. Conductometric titration

The carboxyl content of oxidised cellulose was determined using conductometric titration [43]. 50 mg of dried oxidised samples were hydrolysed using 15 ml of 0.01 M HCl while stirring (400 rpm, 20 min). This suspension was titrated with 0.01 M NaOH until it reached a conductivity level similar to the starting point. While adding the titrant, the samples were stirred for 1 min, and the change in conductivity was recorded. The carboxyl group content (mmol g^{-1}) and degree of oxidation (DO) of the samples were calculated using the following equations [43]:

$$n = (V_2 - V_1) \times c_{NaOH} \quad (1)$$

$$DO = (162 \times n)/(m - 36 \times n) \times 100\% \quad (2)$$

with n being the carboxyl content (mmol g^{-1}), V_1 and V_2 are the volumes of NaOH in the first and second titration endpoint, c_{NaOH} is the NaOH concentration, m is the sample weight, and 36 being the molecular mass difference of the non-oxidised and oxidised cellulose monomer. The conductometric titration curves display distinct endpoints for each sample due to carboxyl groups (-COOH) present (SI, Fig. S5).

3.3. Scanning electron microscopy (SEM)

SEM was carried out using a Zeiss Leo 1530 and TESCAN Clara 2023, working at an acceleration voltage of 5 kV. Morphology and surface topography were detected using secondary electrons and axial detectors with 20,000, 90,000×, and 70,000× magnification, respectively. The samples were prepared on aluminium tape and coated with a 20 nm layer of gold using a sputter coater (BAL-TEC SCD 050).

3.4. Transmission electron microscopy (TEM)

TEM analysis was performed using a FEI Tecnai F20. A sample drop was cast onto a carbon-coated copper TEM grid. All images were taken using an acceleration voltage of 200 kV.

3.5. Conductometric-potentiometric titration

A reliable technique known as conductometric-potentiometric titration is commonly employed to determine the number of primary amine groups in polysaccharide-based materials [44]. The conductometric-potentiometric curves display distinct endpoints for

each sample due to the presence of primary amine groups. The 1st derivative was applied to identify these endpoints (SI, Fig. S9). A given amount of amine-grafted CNFs was suspended in 50 ml DDW, and the pH of the solution was adjusted to 3 using 0.1 M HCl. While stirring (400 rpm, 20 min), the suspension was titrated using 0.01 M NaOH. 10–50 μl of titrant were added in 1 min intervals to the solution while recording pH and conductivity. The amount of primary amine groups ($-NH_2$) on the surface was calculated using the equation below:

$$NH_2 = \left(\left(Y \times 10^{-3} \times (V_1 - V_2) \times M\right)/m\right) \quad (3)$$

with Y being the molar mass of the monomeric unit of fully amine-grafted CNFs (g mol^{-1}), V_1 and V_2 being the volumes of titrant at the equivalent points (ml), M is the concentration of NaOH solution (mol l^{-1}), and m is the weight of the samples used (g).

3.6. Zeta potential measurements

The zeta potential of the samples was analysed at 25 °C using a Malvern Zetasizer Nano Z. All samples were freshly prepared, and their pH was adjusted between 2 and 12 using 0.1 M NaOH solution. To overcome the electric current flow on the particles and to get reliable data, each sample was measured 3 times with 10–20 runs each.

3.7. Gel permeation chromatography (GPC)

GPC, combined with a RI (refractive index) and an ultraviolet (UV) absorbance detector, was used to determine the molar mass distribution of the cellulose samples. Sample preparation followed our previously published protocol [37].

3.8. X-ray photoelectron microscopy (XPS)

For XPS measurements, the powders were pressed into In foil on a Cu sample holder without further treatment. The XPS spectra were recorded using non-monochromatic Mg Kα radiation (1253.6 eV) from the XR-50 X-ray source of the XPS spectrometer (SPECS Surface Nano Analysis GmbH, Berlin, Germany). The pressure in the analyser chamber was 3×10^{-8} mbar or less. The pass energy, E_p, of the PHOIBOS 100 hemispherical energy analyser with multi-channeltron detector was set to 50 eV to record wide energy scans. Multiple narrow scans with higher energy resolution (FWHM = 1.0 eV for Ag $3d_{5/2}$) were recorded at E_p = 13 eV.

Data analysis of the XPS spectra was performed using the software package CasaXPS (version 2.3.25PR1.0) [45]. After subtraction of a linear background, the XPS signals were modelled with a Gaussian-Lorentzian line shape. In the case of multiple components in the 1s spectra of C, N, or O, respectively, the FWHM of the corresponding components was linked and varied as one parameter during the least-squares fitting. The electron binding energies, E_b, were corrected for electrostatic surface charging by setting the C 1s binding energy of aliphatic carbon to 285.0 eV. The experimental uncertainty of the binding energies is ±0.1 eV. Sample atomic concentrations (atom %) were calculated from relative peak intensities using the following empirical sensitivity factors: N 1s/C 1s = 1.70 and O 1s/C 1s = 2.53. The relative error is estimated to be <5 %.

4. Result and discussion

In this study, dinoflagellate-derived native cellulose is first converted to CNFs by a one-step regioselective (C_6) oxidation using TEMPO/NaBr/NaOCl. In a second step, these CNFs are further amine-functionalised with folic acid to enhance their biological affinity. FA-conjugation was performed using a two-step reaction: Initially, the surface carboxyl groups were linked with the small-chain diamineputrescine – which then served as an amine linkage to enable the attachment of the sterically demanding FA. In the third part, FA-grafted CNFs are investigated as potential drug carriers using MB as a model drug.

Table 1
Characterisation results of dinoflagellate-derived CNFs after oxidation and amine-grafting: DO, amount of surface carboxyl groups [COOH], ζ potential, reaction yield, and DP calculated from GPC data. Drug loading efficiency (DLE) is given for amine-grafted samples.

Oxidised samples						
Reaction time	Reagent ratio	DO/ %	[COOH]/ mmol g^{-1}	ζ-Potential/ mV (pH 7)	Yield/ %	DP
1 h	1:0.5	31	1.51	−44.1	86	860
1 h	1:1	35	1.95	−50.2	81	845
1 h	1:2	30	1.6	−44.7	74	764
12 h	1:1	33	1.79	−48.2	55	723
24 h	1:1	32	1.7	−44.0	33	385

Amine-grafted samples						
Reaction time	[$-NH_2$]/ mmol g^{-1}	[-NH-]/ mmol g^{-1}	Yield/ %	ζ-Potential/ mV (pH 7)	M_w/ g mol^{-1}	DLE/ mg g^{-1}
3 h	2	1	43	−13.0	4.23×10^4	21
24 h	8.2	7.8	68	−35.0	1.15×10^5	400

All reaction products (CNFs after oxidation, after putrescine and FA-grafting) were thoroughly characterised by conductometric titration (Table 1 and Figs. S5, S9, S10, S11), zeta potential measurements (Table 1 and SI, Fig. S4), TGA (SI, Table S1), GPC (Table 1), ATR-FTIR (Figs. 1, 3), XPS (Fig. 4, SI, Figs. S13, S14), SEM (Fig. 2), and XRD (SI, Fig. S12).

4.1. Oxidation of dinoflagellate-derived cellulose

One-step TEMPO oxidation was applied to cellulose extracted from the dinoflagellate species *Peridinium* sp. and *P. micans* [37]. The protocol was conducted using different reaction times and reagent ratios. Table 1 summarises the characterisation results of all samples.

The success of the oxidation procedure was confirmed using zeta potential measurements and ATR-FTIR spectroscopy. In addition, the DO and the degree of polymerisation (DP) of the oxidised samples were calculated using conductometric titration (SI, Fig. S5) and GPC analysis.

4.1.1. Zeta potential

As a result of the one-step oxidisation process, the suspension became visibly transparent after 1 h of reaction time (SI, Fig. S6). Non-oxidised dinoflagellate-derived cellulose has a zeta potential of approximately −8 mV (SI, Table S1). After oxidisation, the zeta potential of the transparent samples is significantly shifted to more negative values, ranging from −41 mV to −52 mV (Table 1). In addition, zeta potential analysis at different pHs showed that above a pH value of 8, dinoflagellate-derived CNFs form stable suspensions (SI, Fig. S4).

This notable change in surface charge can be attributed to the introduction of surface carboxyl groups as a consequence of a successful oxidisation process, which converted the CFs into more soluble CNFs.

4.1.2. ATR-FTIR spectroscopy

The transformation of surface hydroxyl into carboxyl groups is also visible in the FTIR spectra of non-oxidised and oxidised samples (Fig. 1). After oxidisation, the surface of the material is predominantly covered with carboxylate ions (in this case, COO^-Na^+). This is evidenced by the band at 1603 cm^{-1} (highlighted in Fig. 1) corresponding to the asymmetric carboxylate (-COO^-) stretching vibration [46]. This band is absent in the non-oxidised samples, which is a strong indicator of successful oxidisation.

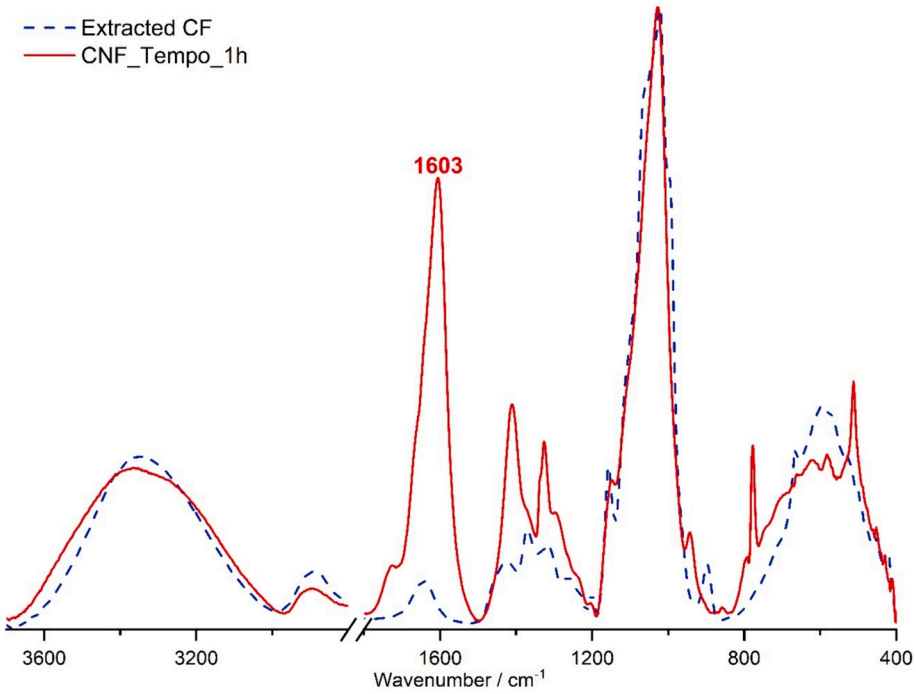

Fig. 1. FTIR spectra of non-oxidised and oxidised dinoflagellate cellulose. Spectra were baseline corrected and normalised to the C-O-C symmetric stretching vibration at 1050 cm^{-1}.

4.1.3. Conductometric titration and GPC analysis

DO of surface carboxyl groups and DP were determined by conductometric titration and GPC analysis. A typical conductometric titration curve is illustrated in the SI (Fig. S5). The highest degree of oxidisation was achieved using a 1:1 M ratio of AGU/NaOCl at pH 10.5 at RT for 1 h. In this case, the number of surface carboxyl groups was 1.95 mmol g^{-1} (DO – 35 %) with an 81 % reaction yield (Table 1).

Increasing the AGU/NaOCl ratio to 1:2 did not increase the number of surface carboxyl groups (Table 1). Instead, the DO significantly decreased to ~30 % (1.6 mmol g^{1} –COOH) and the reaction yield to 74 % (Table 1). A decrease in reaction yield (33 %) and DO (32 %) was also observed for increasing reaction times (from 1 h to 12 and 24 h) at a constant 1:1 NaOCl/AGU ratio (Table 1). This can be explained by the fact that when cellulose samples are exposed to an alkaline environment for an extended period of time, the hydrogen bonds between and within the monomeric units eventually break down [47]. Consequently, as the reaction time or reagent ratio is increased, DP decreases along with DO and reaction yield. For example, if a reaction time of 24 h is used instead of 1 h while maintaining a 1:1 reagent ratio, the DP drops from 845 (1 h) to 385 (24 h) (Table 1). This is a clear indication of increased polymer degradation, which produces short-chain cellulose fragments that are quickly discarded during the washing process.

In conclusion, neither increasing the reaction time nor the NaOCl quantity is necessary for improving the DO in dinoflagellate-derived cellulose. Using a low AGU/NaOCl ratio of 1:1 and a reaction time of only 1 h, the protocol allows to obtain CNFs from dinoflagellate cellulose with higher DO and DP compared to microcrystalline cellulose [47].

4.1.4. Benefits of using dinoflagellate cellulose

The main advantage of using dinoflagellate biomass is that it provides a defacto lignin-free and amorphous cellulose substrate [37]. The amorphous nature of the cellulose of *Peridinium* sp. and *P. micans* simplifies the production of CNFs to one-step TEMPO oxidation, as no additional hydroxyl group activation is required [16]. In other microalgae, complete oxidation of microalgal-derived crystalline cellulose requires 2 h at a temperature of 40 °C after prior surface activation [36]. In our case, the same outcome was achieved in only 1 h at RT with a reaction yield of approximately 80 % (Table 1). An amorphous cellulose substrate is, therefore, highly advantageous for CNF production as it significantly reduces reaction times and reagent ratios compared to crystalline cellulose sources.

4.2. CNF dimensions

The dimensions of the oxidised cellulose product were examined using light (SI, Fig. S7) and electron microscopy (Fig. 2).

4.2.1. SEM/TEM

SEM measurements (Fig. 3a, c) of the oxidised products revealed that the length of the individual fibres varied between 2 and 5 μm, while their widths ranged between 50 and 150 nm (Fig. 3a). These dimensions are characteristic of CNFs derived from microalgae [36].

Due to fibre agglomeration during sample preparation, the number of fibres visible in the TEM was limited. Only small fragments could be observed (Fig. 3b, d), which did not accurately represent the length of the fibres, which were outside the TEM scale. TEM images were, therefore, only used to accurately describe the width of the fibres (Fig. 3b, d), whereas SEM was used to accurately describe the length of the CNFs.

Please note that similar morphologies were also observed in amine-conjugated samples (Fig. 3c, d), with the individual CNFs ranging between ~2–3 μm in length and 50–150 nm in width. These results confirm that the natural cellulose fibres were successfully transformed into CNFs through oxidation, with this nanofibre structure persisting after amine-grafting.

4.3. Amine grafting of dinoflagellate-derived CNFs

A two-step reaction sequence was used for amine grafting. Initially, CNFs were reacted with putrescine to introduce primary amine groups on their surface (reaction scheme in SI, Fig. S2). Next, the putrescine-modified CNFs were conjugated with FA via EDC/NHS coupling (SI, Fig. S3) using different reaction times (3 and 24 h) to increase the reaction yield (Table 1). The success of the amine grafting was confirmed

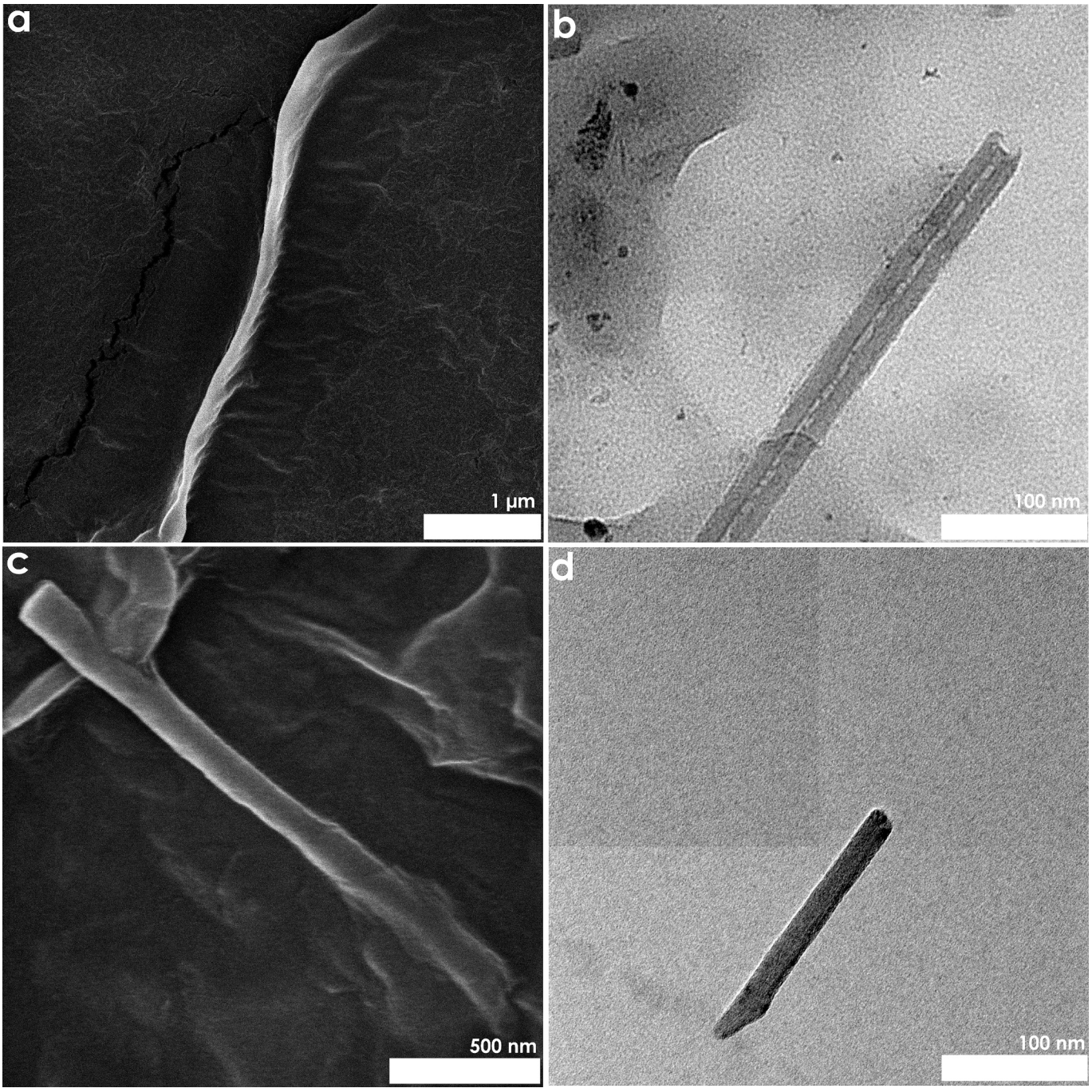

Fig. 2. Morphology of CNFs obtained from dinoflagellate cellulose. High-resolution SEM (a, c) and TEM (b, d) images of CNFs after oxidation (a and b) and FA-grafting (c and d).

using zeta potential measurements, ATR-FTIR spectroscopy, and XPS.

4.3.1. Zeta potential

The putrescine modification significantly increased the zeta potential of the samples, reaching a positive value of +24 mV at a pH of 2 for a 24-hour reaction time (SI, Fig. S8). This can be attributed to the number of NH_2 groups created on the surface of the CNFs, which indicates the success of the putrescine modification (SI, Fig. S8).

After FA-conjugation, the zeta potential of the CNFs shifts to more negative values. Extending the reaction time from 3 to 24 h led to a notable decrease in the zeta potential of the final product, reducing it from +12 mV (SI, Table S1) to −35 mV with a reaction yield of 68 % (Table 1). This zeta potential change demonstrates the successful introduction of negatively charged carboxyl and carbonyl groups via the conjugation of FA. After reaching a pH value of 8, FA-grafted CNFs form stable suspensions (SI, Fig. S8).

4.3.2. ATR-FTIR spectroscopy

Fig. 3 illustrates the spectrum of FA-modified CNFs alongside the spectrum of pure FA, putrescine-modified and oxidised CNF. The most prominent difference between the spectra are the new bands around 1635 cm^{-1} and 1720 cm^{-1} in the FA-conjugated CNFs. The band at 1635 cm^{-1} can be attributed to the amide I stretching vibration [41,46], which shows the successful amine grafting. This is supported by characteristic folic acid bands in the fingerprint region (between ~1200–600 cm^{-1}, dashed lines in Fig. 3). The band at 1720 cm^{-1}

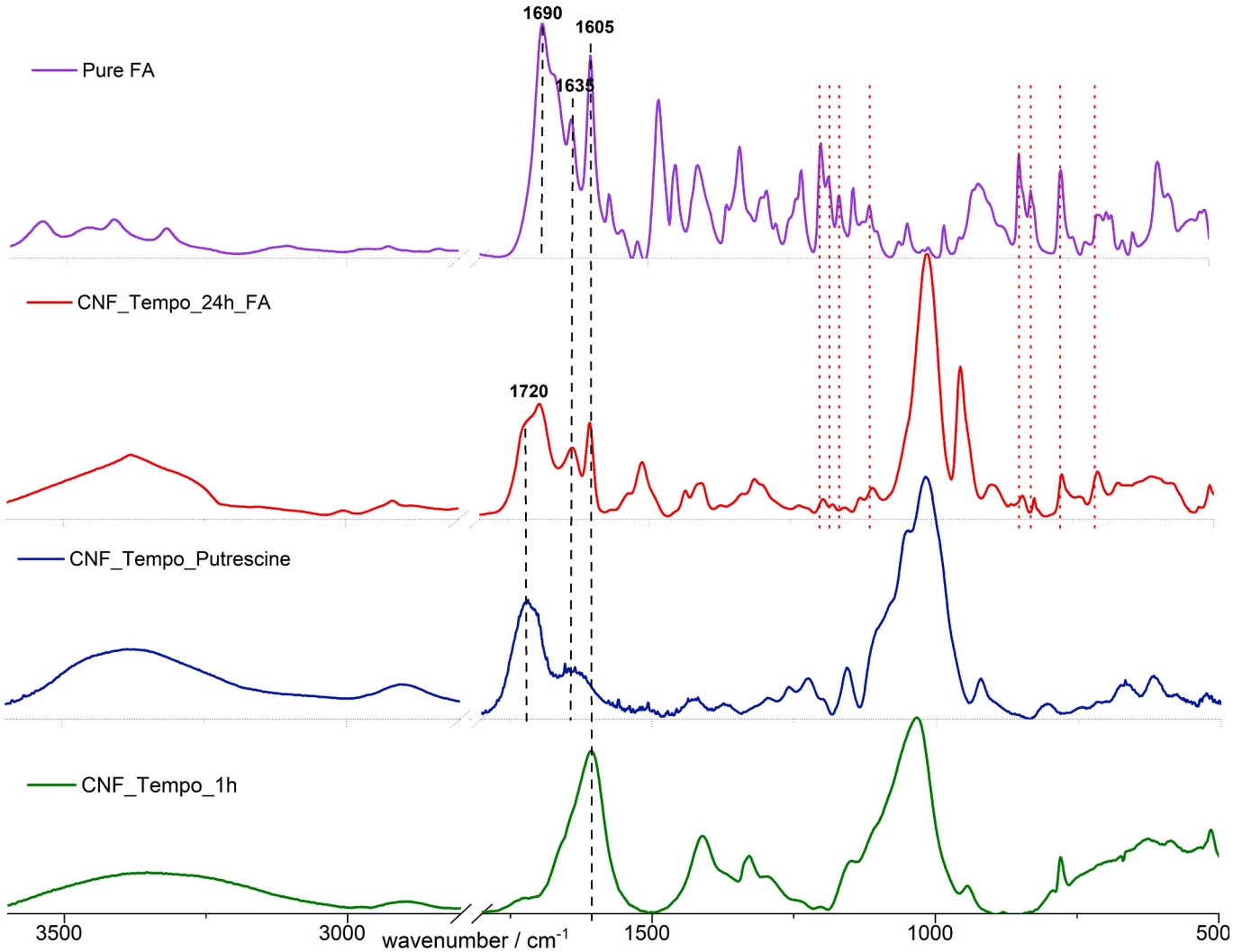

Fig. 3. From top to bottom: FTIR spectrum of pure folic acid (purple), FA-conjugated CNFs (red), putrescine-grafted CNFs (blue), and CNFs after oxidation (green). Spectra were baseline corrected and normalised to the highest band. (For interpretation of the references to colour in this figure legend, the reader is referred to the web version of this article.)

Table 2
Sample composition in atom-% (uncertainty <5 %).

Sample	C	N	O
CNF_Tempo_1h	58	–	42
CNF_Tempo_24h_Putrescine	52	4	44
CNF_Tempo_24h_FA	64	13	23

corresponds to the C═O stretching vibration of COOH, whereas the 1605 cm^{-1} band represents the C═O stretch of COO^- [41,46]. Note that once oxidised, cellulose is completely deprotonated (COO^-Na^+ form), and no band is observed at 1720 cm^{-1}. Amine grafting involves changing the pH and protonating the carboxylate, resulting in the appearance of a band at 1720 cm^{-1}. Overall, the FTIR spectra confirm successful amine conjugation.

4.3.3. XPS

XPS measurements (Table 2, SI, Tables S2, S3) were performed to characterise the surface functional groups of the CNFs after oxidation (SI, Fig. S13) and amine conjugation (Fig. 4; SI, Fig. S14). Oxidised samples were hydrolysed before XPS measurements to eliminate sodium impurities.

The peak areas of the high-resolution spectra (Fig. 4 bottom) were used for quantification, resulting in the surface composition of the samples (Table 2). In addition, curve fitting was applied to these XPS spectra (Fig. 4 bottom) to determine the binding energies and relative concentrations of the corresponding components (Table 2).

In all samples, the C 1s peak shows a fine structure due to different functionalities. The best curve fit was obtained with three components (Fig. 4, SI, Figs. S13, S14, Tables S2, S3): The binding energy E_b at 285.0 eV represents aliphatic/aromatic carbons, the E_b of ~287 eV corresponds to -C-OH groups typical for the cellulose ring structure, and the E_b of ~289 eV belongs to carboxylic carbons. In the oxidised sample, the signal of the carbons with attached hydroxyl groups is dominant (48 %, SI, Table S2). With the introduction of FA, the proportion of aliphatic/aromatic carbons increases significantly (52 %, SI, Table S2).

The O 1s spectra of all samples show a component at 533.0–533.3 eV binding energy. According to reference XPS spectra of various amino acids and peptides, the O 1s signal of C–OH groups and the carboxylic OH group (O=C–OH) occurs at 533.2–533.3 eV [48]. Therefore, these functional groups are present in all investigated samples. In addition to the component at ~533 eV, the O 1s spectrum of reference compounds with a protonated carboxylic group showed a second component at lower binding energy, i.e. at ~532 eV corresponding to the doubly bonded oxygen in the carboxylic group (O=C–OH) [48,49]. The oxygen atoms in deprotonated COO^- have the same environment. Therefore,

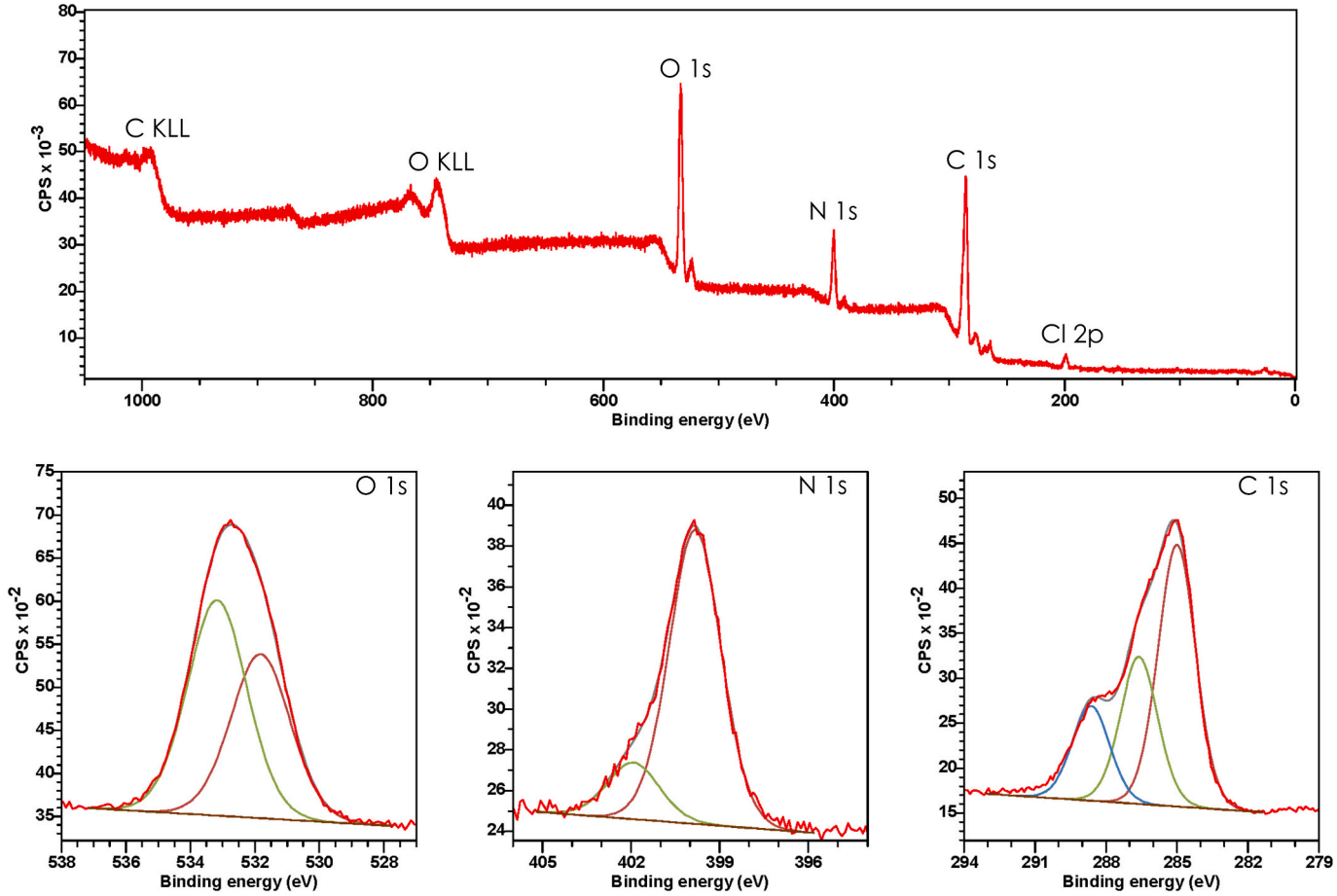

Fig. 4. XPS analysis of FA-conjugated CNFs. Overview scan (top) and narrow scans with higher energy resolution (bottom) with peak fitting for oxygen, nitrogen, and carbon.

only one component with a binding energy of 531.2–531.6 eV is observed in O 1s spectra [48]. The occurrence of an additional O 1s component at 531.3 and 531.8 eV, indicating the presence of COO^- groups in the putrescine-grafted and FA-grafted samples (see Figures and Tables), respectively, seems to be related to the amine conjugation and formation of zwitterionic amine nitrogen (see below). It should be noted that the O 1s component at 531.8 eV in the FA-grafted CNF may also contain a contribution from O=C–OH (~532 eV), which could not be resolved in our XPS measurement.

Evidence for successful amine conjugations is the observation of the N 1 s XPS signal (Fig. 4, SI, Fig. S14). The amount of nitrogen is 4 atom-% for the putrescine-grafted sample and 13 atom-% for the FA-grafted CNFs (Table 2). The fine structure reveals two components at distinct binding energies at 399.8 ± 0.1 eV (amine nitrogen) and 401.8 ± 0.1 eV (protonated nitrogen, NH_3^+) (SI, Table S3) for amine-conjugated samples. For the putrescine-modified sample, primary NH_2 groups (401.8 eV) dominate (~81 %) over the protonated amine nitrogen (399.8 eV, 19 %). The formation of zwitterionic, protonated amine nitrogen agrees with the observation of deprotonated COO^- groups (13 %) in this sample. For the FA-grafted CNF, the N 1 s signal corresponding to secondary and ternary/aromatic amines (399.8 eV) dominates (84 %), and the relative amount of protonated amine nitrogen is only 16 %. This can be explained by the chemical structure of FA, which introduces six secondary and aromatic nitrogen while retaining only one primary amine group (cf. SI, Fig. S3), which could form NH_3^+. The protons are provided by carboxylic groups as indicated by the observation of COO^- in the O 1 s spectrum of the FA-grafted CNF.

Overall, these quantitative XPS measurements provide evidence for the successful formation of amine groups on the CNF surface.

4.3.4. Potentiometric-conductometric titration

To analyse the number of primary amine groups, putrescine and FA-conjugated CNFs were quantitively analysed using the potentiometric conductometric titration method (SI, Figs. S9, S10, S11). The amount of primary amine groups after putrescine modification is illustrated in the SI (Table S1). For the FA-grafted samples, a maximum amount of 8.2 mmol g^{-1} primary amine groups could be achieved by adding 2 mols of FA per mol of -NH_2 surface groups of the putrescine-modified CNFs for 24 h (Table 1). This value is significantly higher than the number of NH_2 groups achieved for MCC by Jelkmann et al. (192–311 μmol g^{-1}) [50]. This can be explained by the amorphous nature of dinoflagellate cellulose, with a large number of accessible OH groups and, consequently, a larger number of accessible carboxylate groups that can be substituted by primary amine groups.

4.3.5. GPC analysis

The GPC analysis showed that the molecular weight of CNFs obtained via amine grafting is approximately 10^5 g mol^{-1} (Table 1). These results are similar to the ones that were obtained for extracted CF [31]. This once again supports the notion that the cellulose polymer chains have not been significantly degraded by the functionalisation process.

4.4. Drug delivery

4.4.1. Drug loading efficiency (DLE)

To assess the capacity of the amine-grafted CNFs to carry drugs, MB was loaded onto the material. MB is structurally similar to commercial anticancer drugs, such as doxorubicin and hydroxyurea and is frequently used to study drug loading and release efficiency of composite materials.

Table 3
Overview: CNFs in drug delivery.

System	Cellulose source	Drug loading/%	Drug release pH	Drug model	Reference
CNF	Dinoflagellates	~100	5.4	MB	This study
Cellulose acetate NF	Commercial	74–95	5.5	Shikonin, akannin	[57]
CNF aerogel	Commercial	18–20	7.4	Bendamustine	[58]
CNF	Lemongrass	20–60	7.4	Camptothecin	[59]
CNF aerogel	Commercial	60–99	6.5–7.4	Doxorubicin	[60]
Cellulose acetate NF	Commercial	84–93	N/A	Naproxen	[61]

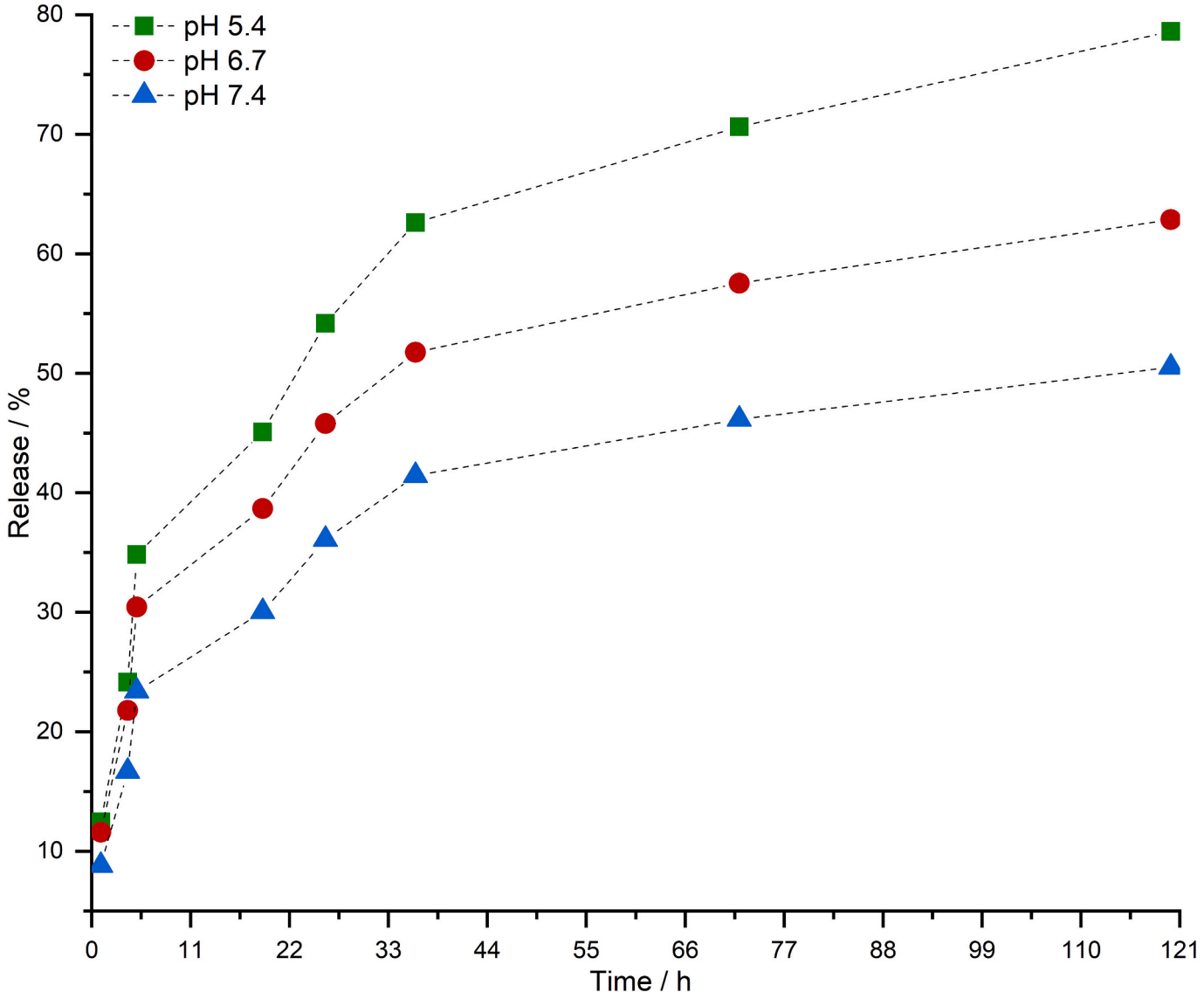

Fig. 5. Drug release: Percentage of released MB in different physiological buffers at pH 5.4 (green, squares), 6.7 (red, circles), and 7.4 (blue, triangles). (For interpretation of the references to colour in this figure legend, the reader is referred to the web version of this article.)

[51]. After surface grafting of dinoflagellate-derived CNFs with primary amine groups, MB can interact with the material through electrostatic interactions [52]. The MB concentration on the sample was determined indirectly by UV/Vis measurements of its concentration in the loading supernatant.

As expected, the FA-conjugation for 3 h shows a low MB loading efficiency of 52 % with 2 mg g^{-1} (Table 1). The maximum amount of MB loaded onto the CNFs was around 99.98 % with 400 mg g^{-1}, achieved within 48 h of MB adsorption and after 24 h of FA reaction time (Table 1). The obtained result is noticeably higher compared to previously published research (Table 3). However, a similar result was observed in 2-hydroxyethylmethylmethacrylate-conjugated CNFs (467.51 mg g^{-1}) from wood cellulose pulp [53].

4.4.2. Drug release

Apart from testing the drug loading efficiency, comprehensive tests were carried out to determine the drug-release properties of the samples. Drug release was observed over 1 week, with samples taken at varying intervals (Fig. 5). A substantial release of MB was observed within the initial 12 h (Fig. 5). Following this initial burst release, the release

continued at a gradually reducing rate.

When comparing the different environments, in the more alkaline environments at pH 6.7 and 7.4, the release of MB is less pronounced compared to the more acidic environment at pH 5.4. In alkaline conditions, the surface carboxyl groups remain negatively charged, leading to a strong electrostatic interaction between MB and the CNF surface. Conversely, in a more acidic environment, the surface groups of the CNFs become protonated, resulting in MB repulsion. These findings align with prior research studies [54–56]. For instance, 5-fluorouracil-doped CNF poly(N-isopropylacrylamide) hybrid microspheres showed an 89 % cumulative release within 1 h at 22 °C [54]; doxorubicin-doped 3D CNF/polyethyleneimine-N/isopropylacrylamide aerogels showed 59.45 % cumulative release within 8 h at pH 3 and 37 °C [55]; and sodium salicylate-doped CNFs/polyethyleneimine aerogels showed 78.49 % cumulative drug release at pH 7.4 within 6 h [56]. Such controlled drug release patterns are highly advantageous in the context of a potential drug delivery system as they reduce the risk of sudden and excessive drug release over a short timeframe, which is critical in pharmaceutical applications [6].

5. Conclusion

This study demonstrates an innovative method for converting amorphous cellulose derived from dinoflagellates into CNFs using a simple one-step oxidation process using TEMPO/NaOCl/NaCl. Our findings provide compelling evidence that dinoflagellate-derived cellulose fibres can be easily converted into CNFs without the need for prior surface hydroxyl group activation. The CNFs obtained were 1–5 μm in length and 50–150 nm in width.

The optimised oxidation process (1:1 ratio of AGU/NaOCl, 1 h at RT, pH 10.5) resulted in a DO of 35 % and a reaction yield of 81 % while maintaining a reliable degree of polymerisation (DP = 845).

By skipping the pre-surface activation step and because of its enhanced accessibility, the production of CNFs from amorphous dinoflagellate cellulose is less time, energy, and chemical-consuming than comparable crystalline cellulose sources, making the process straightforward and more sustainable.

The high degree of oxidation achieved for dinoflagellate CNFs allowed for a successful functionalisation with primary amine groups, which strongly enhances their biological affinity. Surface modification with primary amine groups using sequential treatment with putrescine and folic acid (24 h, pH 7.5–8, RT) resulted in 8 mmol g^{-1} NH_2 per gram of CNFs. The quantitative and qualitative representation of surface functional groups (-COOH, -NH_2) was additionally supported by XPS analyses. The atomic wt% of N in FA-conjugated samples was 14, indicating successful amine conjugation.

In a proof-of-principle drug delivery test, the amine-functionalised CNFs demonstrate an impressive drug loading capacity (~400 mg g^{-1}) with a controlled drug release for up to 120 h, indicating their potential in biomedical applications. Further investigations using pharmaceutical drug molecules are planned to reveal the applicability of dinoflagellate CNFs under more realistic drug-delivery conditions.

Overall, these results show that the unique amorphous nature of dinoflagellate cellulose is beneficial for the production and functionalisation of CNFs. Our findings suggest that dinoflagellate-derived CNFs provide an eco-friendly platform that can be easily functionalised for various applications, especially for drug delivery. This proof of principle study paves the way for the development and application of microalgae-based CNFs.

CRediT authorship contribution statement

Amina Alizade: Conceptualization, Data curation, Formal analysis, Investigation, Methodology, Software, Validation, Visualization, Writing – original draft, Writing – review & editing. **Tobias Reich:** Investigation, Software, formal analysis (XPS), Writing – review & editing. **Anne Jantschke:** Funding acquisition, Supervision, Writing – review & editing, Project administration, Conceptualization, Ressources.

Declaration of competing interest

The authors declare the following financial interests/personal relationships which may be considered as potential competing interests: Anne Jantschke reports financial support was provided by German Research Foundation. Amina Alizade reports financial support was provided by German Research Foundation. If there are other authors, they declare that they have no known competing financial interests or personal relationships that could have appeared to influence the work reported in this paper.

Acknowledgements

Amina Alizade, Anne Jantschke and this project were financially supported by the German Research Foundation (DFG) [JA 2659/3-1]. The authors would like to acknowledge Mr. R. Meffert for his help with the use of the XRD equipment. We also thank Mr. T. Haeger for his kind advice on the use of the ATR-FTIR and TGA. In addition, we would like to thank Mr. M. Hansen for the conductometric probe and Mrs. G. Borngässer/Timo Willershäuser for providing the UV/Vis spectrometer. Moreover, we thank Mr. J. Leitner (Max Plank Institute for Chemistry Mainz) for the SEM measurements and Mr. Ingo Lieberwirth (Department of Physical Chemistry of Polymers, Max Plank Institute for Polymer Research Main) for the TEM measurements. Special thanks to Mrs. S. Morsbach, Mr. L. Caire da Silva, Mrs. C. Rosenauer and Mr. Sh. P. Chali (Department of Physical Chemistry of Polymers, Max Plank Institute for Polymer Research Mainz) for providing the GPC and zeta potential equipment.

Appendix A. Supplementary data

Supplementary data to this article can be found online at https://doi.org/10.1016/j.ijbiomac.2024.132804.

References

[1] O. Nechyporchuk, M.N. Belgacem, J. Bras, Production of cellulose nanofibrils: a review of recent advances, Ind. Crop. Prod. 93 (2016) 2–25, https://doi.org/10.1016/j.indcrop.2016.02.016.
[2] J. Moohan, S.A. Stewart, E. Espinosa, A. Rosal, A. Rodríguez, E. Larrañeta, R. F. Donnelly, J. Domínguez-Robles, Cellulose nanofibers and other biopolymers for biomedical applications. A review, Appl. Sci. 10 (2020) 65, https://doi.org/10.3390/app10010065.
[3] A. Etale, A.J. Onyianta, S.R. Turner, S.J. Eichhorn, Cellulose: a review of water interactions, applications in composites, and water treatment, Chem. Rev. 123 (2023) 2016–2048, https://doi.org/10.1021/acs.chemrev.2c00477.
[4] T. Yi, H. Zhao, Q. Mo, D. Pan, Y. Liu, L. Huang, H. Xu, B. Hu, H. Song, From cellulose to cellulose nanofibrils-a comprehensive review of the preparation and modification of cellulose nanofibrils, Materials (Basel) 13 (2020), https://doi.org/10.3390/ma13225062.
[5] S. Sepahvand, H. Kargarzadeh, M. Jonoobi, A. Ashori, S. Ismaeilimoghadam, R. T. Varghese, C.J. Chirayl, B. Azimi, S. Danti, Recent developments in nanocellulose-based aerogels as air filters: a review, Int. J. Biol. Macromol. 246 (2023) 125721, https://doi.org/10.1016/j.ijbiomac.2023.125721.
[6] Y. Huo, Y. Liu, M. Xia, H. Du, Z. Lin, B. Li, H. Liu, Nanocellulose-based composite materials used in drug delivery systems, Polymers (Basel) 14 (2022), https://doi.org/10.3390/polym14132648.
[7] N.V. Puppala, P. Doddipatla, G. Mohannath, Use of nanocellulose in the intracellular delivery of biological and non-biological drugs: a review, Cellulose 30 (2023) 1335–1354, https://doi.org/10.1007/s10570-022-04977-w.
[8] N. Raghav, M.R. Sharma, J.F. Kennedy, Nanocellulose: a mini-review on types and use in drug delivery systems, Carbohydrate Polymer Technologies and Applications 2 (2021) 100031, https://doi.org/10.1016/j.carpta.2020.100031.
[9] H. He, M. Cheng, Y. Liang, H. Zhu, Y. Sun, D. Dong, S. Wang, Intelligent cellulose nanofibers with excellent biocompatibility enable sustained antibacterial and drug release via a pH-responsive mechanism, J. Agric. Food Chem. 68 (2020) 3518–3527, https://doi.org/10.1021/acs.jafc.9b06588.
[10] S. Sepahvand, A. Ashori, M. Jonoobi, Application of cellulose nanofiber as a promising air filter for adsorbing particulate matter and carbon dioxide, Int. J. Biol. Macromol. 244 (2023) 125344, https://doi.org/10.1016/j.ijbiomac.2023.125344.

[11] J. Shojaeiarani, D.S. Bajwa, S. Chanda, Cellulose nanocrystal based composites: a review, Composites Part C: Open Access 5 (2021) 100164, https://doi.org/10.1016/j.jcomc.2021.100164.
[12] S. Sepahvand, M. Jonoobi, A. Ashori, D. Rabie, F. Gauvin, H.J.H. Brouwers, Q. Yu, T.H. Mekonnen, Modified cellulose nanofibers aerogels as a novel air filters; synthesis and performance evaluation, Int. J. Biol. Macromol. 203 (2022) 601–609, https://doi.org/10.1016/j.ijbiomac.2022.01.156.
[13] B. Azimi, S. Sepahvand, S. Ismaeilimoghadam, H. Kargarzadeh, A. Ashori, M. Jonoobi, S. Danti, Application of cellulose-based materials as water purification filters; a state-of-the-art review, J. Polym. Environ. 32 (2024) 345–366, https://doi.org/10.1007/s10924-023-02989-6.
[14] A.K. Vipin, B. Fugetsu, I. Sakata, A. Isogai, M. Endo, M. Li, M.S. Dresselhaus, Cellulose nanofiber backboned Prussian blue nanoparticles as powerful adsorbents for the selective elimination of radioactive cesium, Sci. Rep. 6 (2016) 37009, https://doi.org/10.1038/srep37009.
[15] M. Rakib Hasan Khan, R. Shankar Hazra, G. Nair, J. Mohammad, L. Jiang, K. Reindl, M. Khalid Jawed, S. Ganai, M. Quadir, Cellulose nanofibers as scaffold-forming materials for thin film drug delivery systems, Int. J. Pharm. 627 (2022) 122189, https://doi.org/10.1016/j.ijpharm.2022.122189.
[16] M. Ioelovich, Preparation, characterization and application of amorphized cellulose-a review, Polymers (Basel) 13 (2021), https://doi.org/10.3390/polym13244313.
[17] A. Kafy, H.C. Kim, L. Zhai, J.W. Kim, T.J. van Hai, J. Kim Kang, Cellulose long fibers fabricated from cellulose nanofibers and its strong and tough characteristics, Sci. Rep. 7 (2017) 17683, https://doi.org/10.1038/s41598-017-17713-3.
[18] Y. Lu, Q. He, G. Fan, Q. Cheng, G. Song, Extraction and modification of hemicellulose from lignocellulosic biomass: a review, Green Processes Synth. 10 (2021) 779–804, https://doi.org/10.1515/gps-2021-0065.
[19] C. Ververis, K. Georghiou, N. Christodoulakis, P. Santas, R. Santas, Fiber dimensions, lignin and cellulose content of various plant materials and their suitability for paper production, Ind. Crop. Prod. 19 (2004) 245–254, https://doi.org/10.1016/j.indcrop.2003.10.006.
[20] X. Jin, X. Chen, C. Shi, M. Li, Y. Guan, C.Y. Yu, T. Yamada, E.J. Sacks, J. Peng, Determination of hemicellulose, cellulose and lignin content using visible and near infrared spectroscopy in Miscanthus sinensis, Bioresour. Technol. 241 (2017) 603–609, https://doi.org/10.1016/j.biortech.2017.05.047.
[21] M. Mićić, Sample Preparation Techniques for Soil, Plant, and Animal Samples, Humana Press, New York, NY, 2016.
[22] D. Watkins, M. Nuruddin, M. Hosur, A. Tcherbi-Narteh, S. Jeelani, Extraction and characterization of lignin from different biomass resources, J. Mater. Res. Technol. 4 (2015) 26–32, https://doi.org/10.1016/j.jmrt.2014.10.009.
[23] H. Seddiqi, E. Oliaei, H. Honarkar, J. Jin, L.C. Geonzon, R.G. Bacabac, J. Klein-Nulend, Cellulose and its derivatives: towards biomedical applications, Cellulose 28 (2021) 1893–1931, https://doi.org/10.1007/s10570-020-03674-w.
[24] H.N. Abdelhamid, A.P. Mathew, Cellulose-based nanomaterials advance biomedicine: a review, Int. J. Mol. Sci. 23 (2022), https://doi.org/10.3390/ijms23105405.
[25] I. Hamed, The evolution and versatility of microalgal biotechnology: a review, Compr. Rev. Food Sci. Food Saf. 15 (2016) 1104–1123, https://doi.org/10.1111/1541-4337.12227.
[26] S. Baba Hamed, M.B. BabaHamed, S. Kassouar, S.M.E.A. Abi Ayad, Physicochemical analysis of cellulose from microalgae Nannochloropsis gaditana, Afr. J. Biotechnol. 15 (2016) 1201–1207.
[27] I.L. Ross, S. Shah, B. Hankamer, N. Amiralian, Microalgal nanocellulose - opportunities for a circular bioeconomy, Trends Plant Sci. 26 (2021) 924–939, https://doi.org/10.1016/j.tplants.2021.05.004.
[28] K. Hwang, G.-J. Kwon, J. Yang, M. Kim, W.J. Hwang, W. Youe, D.-Y. Kim, Chlamydomonas angulosa (green alga) and Nostoc commune (blue-green alga) microalgae-cellulose composite aerogel beads: manufacture, physicochemical characterization, and cd (II) adsorption, Materials (Basel) 11 (2018), https://doi.org/10.3390/ma11040562.
[29] N. Wahlström, U. Edlund, H. Pavia, G. Toth, A. Jaworski, A.J. Pell, F.X. Choong, H. Shirani, K.P.R. Nilsson, A. Richter-Dahlfors, Cellulose from the green macroalgae Ulva lactuca: isolation, characterization, optotracing, and production of cellulose nanofibrils, Cellulose 27 (2020) 3707–3725, https://doi.org/10.1007/s10570-020-03029-5.
[30] Z. Xiang, W. Gao, L. Chen, W. Lan, J.Y. Zhu, T. Runge, A comparison of cellulose nanofibrils produced from Cladophora glomerata algae and bleached eucalyptus pulp, Cellulose 23 (2016) 493–503, https://doi.org/10.1007/s10570-015-0840-7.
[31] E. Zanchetta, E. Damergi, B. Patel, T. Borgmeyer, H. Pick, A. Pulgarin, C. Ludwig, Algal cellulose, production and potential use in plastics: challenges and opportunities, Algal Res. 56 (2021) 102288, https://doi.org/10.1016/j.algal.2021.102288.
[32] A. Mihranyan, Cellulose from cladophorales green algae: from environmental problem to high-tech composite materials, J. Appl. Polym. Sci. 119 (2011) 2449–2460, https://doi.org/10.1002/app.32959.
[33] R.D. Preston, J. Cronshaw, Constitution of the fibrillar and non-fibrillar components of the walls of Valonia ventricosa, Nature 181 (1958) 248–250, https://doi.org/10.1038/181248a0.
[34] R. Madadi, H. Maljaee, L.S. Serafim, S.P.M. Ventura, Microalgae as contributors to produce biopolymers, Mar. Drugs 19 (2021), https://doi.org/10.3390/md19080466.
[35] F. Khavari, M. Saidijam, M. Taheri, F. Nouri, Microalgae: therapeutic potentials and applications, Mol. Biol. Rep. 48 (2021) 4757–4765, https://doi.org/10.1007/s11033-021-06422-w.
[36] H.-R. Lee, K. Kim, S.C. Mun, Y.K. Chang, S.Q. Choi, A new method to produce cellulose nanofibrils from microalgae and the measurement of their mechanical strength, Carbohydr. Polym. 180 (2018) 276–285, https://doi.org/10.1016/j.carbpol.2017.09.104.
[37] A. Alizade, A. Jantschke, Dinoflagellates as sustainable cellulose source: cultivation, extraction, and characterization, Int. J. Biol. Macromol. 242 (2023) 125116, https://doi.org/10.1016/j.ijbiomac.2023.125116.
[38] L.C. Morrill, A.R. Loeblich, Ultrastructure of the dinoflagellate amphiesma, Int. Rev. Cytol. 82 (1983) 151–180, https://doi.org/10.1016/S0074-7696(08)60825-6.
[39] A.C.M. Kwok, W.S. Chan, J.T.Y. Wong, dinoflagellate amphiesmal dynamics: cell wall deposition with ecdysis and cellular growth, Mar. Drugs 21 (2023), https://doi.org/10.3390/md21020070.
[40] A. Isogai, T. Saito, H. Fukuzumi, TEMPO-oxidized cellulose nanofibers, Nanoscale 3 (2011) 71–85, https://doi.org/10.1039/C0NR00583E.
[41] S.-J. Yang, F.-H. Lin, K.-C. Tsai, M.-F. Wei, H.-M. Tsai, J.-M. Wong, M.-J. Shieh, Folic acid-conjugated chitosan nanoparticles enhanced protoporphyrin IX accumulation in colorectal cancer cells, Bioconjug. Chem. 21 (2010) 679–689, https://doi.org/10.1021/bc9004798.
[42] A. Hussain, J. Li, J. Wang, F. Xue, Y. Chen, T. Bin Aftab, D. Li, Hybrid monolith of graphene/TEMPO-oxidized cellulose nanofiber as mechanically robust, highly functional, and recyclable adsorbent of methylene blue dye, J. Nanomater. 2018 (2018) 1–12, https://doi.org/10.1155/2018/5963982.
[43] Z. Tang, W. Li, X. Lin, H. Xiao, Q. Miao, L. Huang, L. Chen, H. Wu, TEMPO-oxidized cellulose with high degree of oxidation, Polymers (Basel) 9 (2017), https://doi.org/10.3390/polym9090421.
[44] L. Pérez-Álvarez, L. Ruiz-Rubio, J.L. Vilas-Vilela, Determining the deacetylation degree of chitosan: opportunities to learn instrumental techniques, J. Chem. Educ. 95 (2018) 1022–1028, https://doi.org/10.1021/acs.jchemed.7b00902.
[45] N. Fairley, V. Fernandez, M. Richard-Plouet, C. Guillot-Deudon, J. Walton, E. Smith, D. Flahaut, M. Greiner, M. Biesinger, S. Tougaard, D. Morgan, J. Baltrusaitis, Systematic and collaborative approach to problem solving using X-ray photoelectron spectroscopy, Applied Surface Science Advances 5 (2021) 100112, https://doi.org/10.1016/j.apsadv.2021.100112.
[46] D.A. Long, Infrared and Raman characteristic group frequencies. Tables and charts George Socrates John Wiley and Sons, Ltd, Chichester, third edition, 2001. Price £135, J. Raman Spectrosc. 35 (2004) 905, https://doi.org/10.1002/jrs.1238.
[47] M. Wohlert, T. Benselfelt, L. Wågberg, I. Furó, L.A. Berglund, J. Wohlert, Cellulose and the role of hydrogen bonds: not in charge of everything, Cellulose 29 (2022) 1–23, https://doi.org/10.1007/s10570-021-04325-4.
[48] J.S. Stevens, A.C. de Luca, M. Pelendritis, G. Terenghi, S. Downes, S.L. M. Schroeder, Quantitative analysis of complex amino acids and RGD peptides by X-ray photoelectron spectroscopy (XPS), Surf. Interface Anal. 45 (2013) 1238–1246, https://doi.org/10.1002/sia.5261.
[49] A. Artemenko, A. Shchukarev, P. Štenclová, T. Wågberg, J. Segervald, X. Jia, A. Kromka, Reference XPS spectra of amino acids, IOP Conf. Ser.: Mater. Sci. Eng. 1050 (2021) 12001, https://doi.org/10.1088/1757-899X/1050/1/012001.
[50] M. Jelkmann, C. Menzel, R.A. Baus, P. Ausserhofer, D. Baecker, R. Gust, A. Bernkop-Schnürch, Chitosan: the one and only? aminated cellulose as an innovative option for primary amino groups containing polymers, Biomacromolecules 19 (2018) 4059–4067, https://doi.org/10.1021/acs.biomac.8b01069.
[51] W. Treesuppharat, P. Rojanapanthu, C. Siangsanoh, H. Manuspiya, S. Ummartyotin, Synthesis and characterization of bacterial cellulose and gelatin-based hydrogel composites for drug-delivery systems, Biotechnol. Rep. (Amst.) 15 (2017) 84–91, https://doi.org/10.1016/j.btre.2017.07.002.
[52] D. da Silva Perez, S. Montanari, M.R. Vignon, TEMPO-mediated oxidation of cellulose III, Biomacromolecules 4 (2003) 1417–1425, https://doi.org/10.1021/bm034144s.
[53] E. Oyarce, P. Cantero-López, O. Yañez, K. Roa, A. Boulett, G.D.C. Pizarro, Y. Zhang, C. Xu, S. Willför, J. Sánchez, Nanocellulose bio-based composites for the removal of methylene blue from water: an experimental and theoretical exploration, J. Mol. Liq. 357 (2022) 119089, https://doi.org/10.1016/j.molliq.2022.119089.
[54] F. Zhang, W. Wu, X. Zhang, X. Meng, G. Tong, Y. Deng, Temperature-sensitive poly-NIPAm modified cellulose nanofibril cryogel microspheres for controlled drug release, Cellulose 23 (2016) 415–425, https://doi.org/10.1007/s10570-015-0799-4.
[55] Y. Liang, H. Zhu, L. Wang, H. He, S. Wang, Biocompatible smart cellulose nanofibres for sustained drug release via pH and temperature dual-responsive mechanism, Carbohydr. Polym. 249 (2020) 116876, https://doi.org/10.1016/j.carbpol.2020.116876.
[56] J. Zhao, C. Lu, X. He, X. Zhang, W. Zhang, X. Zhang, Polyethylenimine-grafted cellulose nanofibril aerogels as versatile vehicles for drug delivery, ACS Appl. Mater. Interfaces 7 (2015) 2607–2615, https://doi.org/10.1021/am507601m.
[57] K.N. Kontogiannopoulos, A.N. Assimopoulou, I. Tsivintzelis, C. Panayiotou, V. P. Papageorgiou, Electrospun fiber mats containing shikonin and derivatives with potential biomedical applications, Int. J. Pharm. 409 (2011) 216–228, https://doi.org/10.1016/j.ijpharm.2011.02.004.
[58] J. Bhandari, H. Mishra, P.K. Mishra, R. Wimmer, F.J. Ahmad, S. Talegaonkar, Cellulose nanofiber aerogel as a promising biomaterial for customized oral drug delivery, Int. J. Nanomedicine 12 (2017) 2021–2031, https://doi.org/10.2147/IJN.S124318.
[59] P. Kumari, A. Meena, Application of enzyme-mediated cellulose nanofibers from lemongrass waste for the controlled release of anticancer drugs, Environ. Sci.

Pollut. Res. Int. 28 (2021) 46343–46355, https://doi.org/10.1007/s11356-020-08358-3.

[60] N. Alizadeh, V. Akbari, M. Nurani, A. Taheri, Preparation of an injectable doxorubicin surface modified cellulose nanofiber gel and evaluation of its anti-tumor and anti-metastasis activity in melanoma, Biotechnol. Prog. 34 (2018) 537–545, https://doi.org/10.1002/btpr.2598.

[61] S. Tungprapa, I. Jangchud, P. Supaphol, Release characteristics of four model drugs from drug-loaded electrospun cellulose acetate fiber mats, Polymer 48 (2007) 5030–5041, https://doi.org/10.1016/j.polymer.2007.06.061.